LEGIBILITY NOTICE

A major purpose of the Technical Information Center is to provide the broadest dissemination possible of information contained in DOE's Research and Development Reports to business, industry, the academic community, and federal, state and local governments.

Although a small portion of this report is not reproducible, it is being made available to expedite the availability of information on the research discussed herein.

LA-UR -90-1433

LA-UR--90-1433

DE90 010615

Los Alamos National Laboratory is operated by the University of California for the United States Department of Energy under contract W-7405-ENG-36.

TITLE: REALISTIC WARHEAD AND BLAST SHIELD TESTING OF CHEMICAL ENERGY WARHEAD SYSTEMS FOR ADVANCED ANTITANK MISSILES

AUTHOR(S): David B. Fradkin, Lawrence M. Hull, and Gary W. Laabs

SUBMITTED TO: Proceedings of the Test Technology Symposium III, 19-21 March 1990, Laurel, Maryland (Science and Technology Corporation, Hampton, Virginia)

DISCLAIMER

Los Alamos Los Alamos National Laboratory
Los Alamos, New Mexico 87545

FORM NO 836 R4

REALISTIC WARHEAD AND BLAST SHIELD TESTING OF CHEMICAL ENERGY TANDEM WARHEAD SYSTEMS FOR ADVANCED ANTITANK MISSILES

David B. Fradkin, Lawrence M. Hull, and Gary W. Laabs

Los Alamos National Laboratory
Los Alamos, NM 87545, USA

ABSTRACT

The results of dynamic sled track performance testing of advanced tandem configuration shaped-charge warheads against multiple-reactive-element tank armors are presented. Tandem configurations utilizing both currently fielded and experimental shaped-charge warheads were tested. Sled velocities used were between 400 and 1100 ft/s (Mach number 0.35 to 0.95), typical of the terminal approach velocity of TOW-type antitank missiles. High-speed motion pictures (5000 frames/s) of the sled in operation and a typical "mock missile" warhead package approaching the target are shown. Details of the sled design and fabrication and of the warhead package design and fabrication are presented. Sled track instrumentation is discussed. This instrumentation includes foil make/break switches and associated time interval meters (TIM) and digital delay units (DDU), magnetic Hall-effect transistors for measuring sled trajectory, and flash x rays (FXR). Methods for timing the x rays are presented. Schematic functional diagrams of the experimental setups are also given. Evidence of the ability to accurately time the delay between precursor and main warheads for even very long time delays are presented.

FXR pictures illustrate the dynamics of the interaction of the jets with various target elements. The interaction dynamics of the jets is discussed in relation to the overall penetration performance of the tandem warhead. The use of x-ray fluorescence spectroscopy to help diagnose interaction dynamics is illustrated.

The results of a test utilizing the missile propulsion rocket motor as a blast shield is presented. FXR and microwave interferometry were used to track the axial movement of the motor as a function of time. The results show the effectiveness of the motor as a blast shield in tandem designs where the motor is placed between the precursor and main charges. Confirmation of this result in full-up sled tests is also discussed.

1. INTRODUCTION

The goal of this program is to develop a shaped-charge tandem warhead configuration that is capable of defeating robust multiple-reactive-element heavy armors. Such an armor is shown schematically in Fig. 1. To defeat such an armor, two warheads are used. The first shaped-charge warhead, the precursor, should detonate both of the reactive packs. The second warhead is detonated sometime later, when the reactive pack tamper and flyer plates have cleared the shot line or are moving at low velocity so they do not substantially disturb the jet. This jet then attacks the main hull armor. A typical warhead arrangement is shown in Fig. 2.

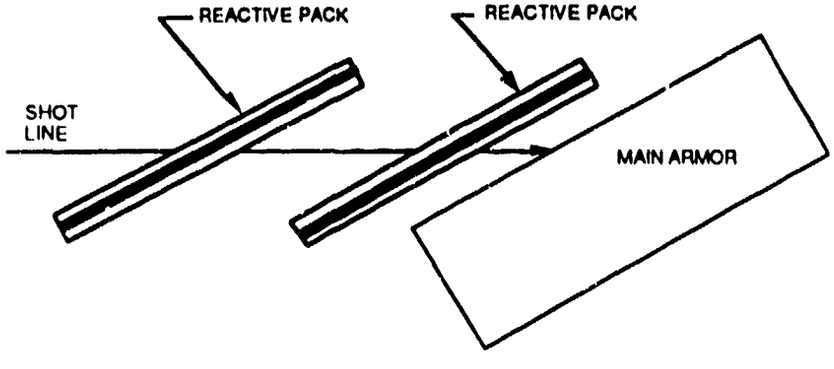

Figure 1. Typical multiple-reactive-pack armor.

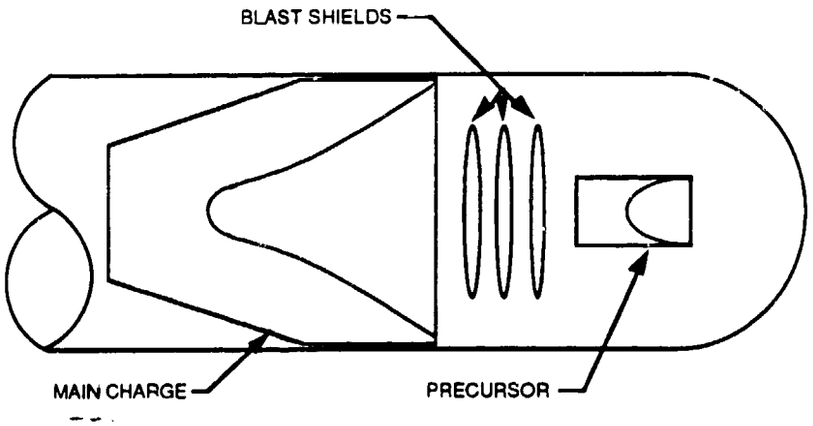

Figure 2. Typical tandem warhead configuration.

In such an arrangement, a blast shield must be placed between the precursor and main charges to protect the main charge during the often substantial time delay between the firing of the two warheads. Our goal in this study was to test warhead configurations that could be used in advanced TOW-type antitank missiles. To this end, we looked at various combinations of fielded and developmental warheads. As far as blast shield designs were concerned, we wished to minimize any parasitic weight of the blast shield. We therefore wanted to test the use of the TOW rocket motor itself as a substantial element of the blast shield system.

2. BLAST SHIELD STUDIES

2.1 USE OF TOW MOTOR AS BLAST SHIELD

Figure 3 shows the experimental arrangement used to test the concept of using the TOW motor as a substantial element of the blast shield system.

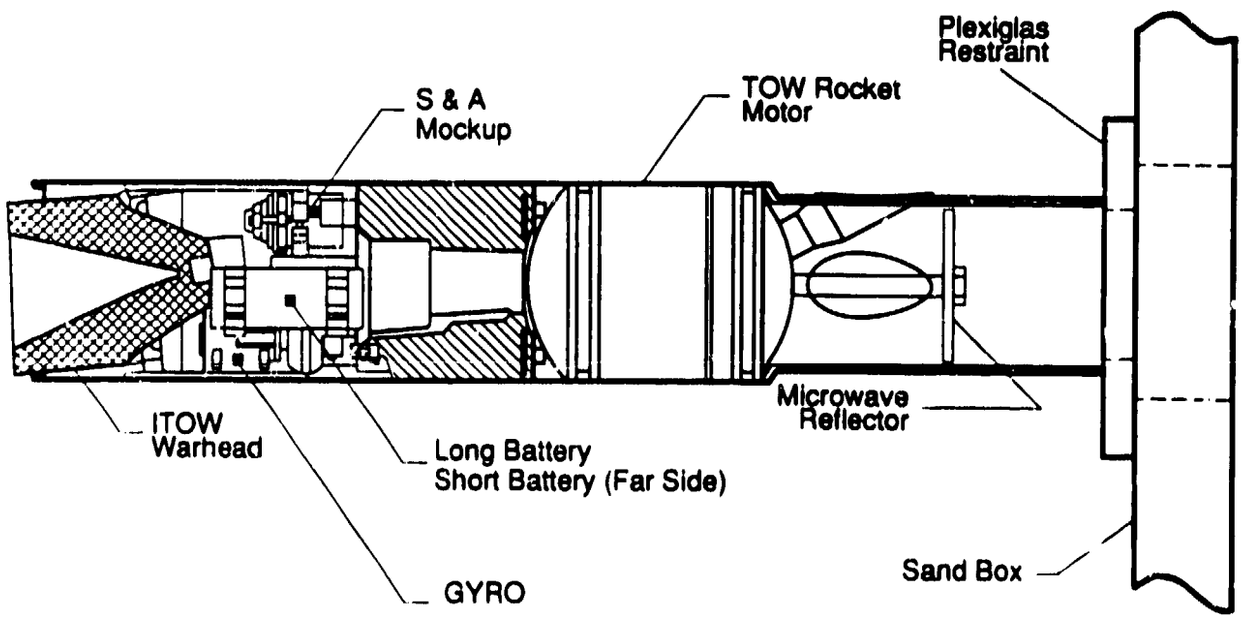

Figure 3. TOW motor blast shield test assembly.

The missile safe-and-arm device, and the gyro, batteries, and circuit boards also aided in blast shielding. To act as an effective blast shield, the TOW motor must maintain mechanical integrity and not move backward into the rear warhead during the period between the firing of the precursor and main warheads. Diagnostics used to determine motor integrity and position were three 450-keV flash x rays and an 8.0-GHz microwave interferometer (McCall et al., 1985). A Lucite disk covered on the back surface with aluminum foil was supported from the back of the TOW motor, just behind the nozzles, to act as a reflector for the microwaves. To simulate the inertia to solid-body rearward motion of the actual missile

provided by the launch motor, the back of our "mock" missile was butted up against a polymethylmethacrylate (PMMA) plate, which was restrained from rearward motion by a sandbox. Holes through the sandbox and PMMA plate allowed the microwaves to reach and return from the reflector. Figure 4 is a photograph of the assembly with the rear missile-skin section removed to show the microwave reflector. Figure 5 shows the arrangement of the microwave interferometer. The interferometer is a microwave analog of an optical Michelson interferometer. The results of this experiment are shown in Figs. 6 and 7. Figure 6 shows the reduced data from the microwave interferometer. A displacement of about 30 mm is observed 1500 μs after the ITOW warhead was detonated. Figure 7 is a triple-exposure radiograph of the event. Exposures were taken at 250 μs, 750 μs, and 1500 μs after warhead detonation. The good mechanical integrity of the TOW motor during the entire time duration is evident. The rearward movement of the motor can be determined from the position of the nozzle fins and the microwave reflector. At 1500 μs, a displacement of about 30 mm is observed, in excellent agreement with the microwave interferometer data. These results gave us confidence that the TOW motor would act as an effective blast shield for precursor warheads with explosive weights as high as that of the ITOW (2700 g of LX-14). Many of our tandem warhead configurations thus used the TOW motor as the main blast shield with a Mincel #12 foam cone, weighing only 89 g placed in front of the motor (personal communication, Walters, W., 1989, U.S. Army Ballistics Research Laboratory). The efficacy of this design is shown in Fig. 8, which is a 2.3-MeV radiograph obtained during a dynamic sled test showing the TOW motor and main warhead more than 2000 μs after the precursor was detonated.

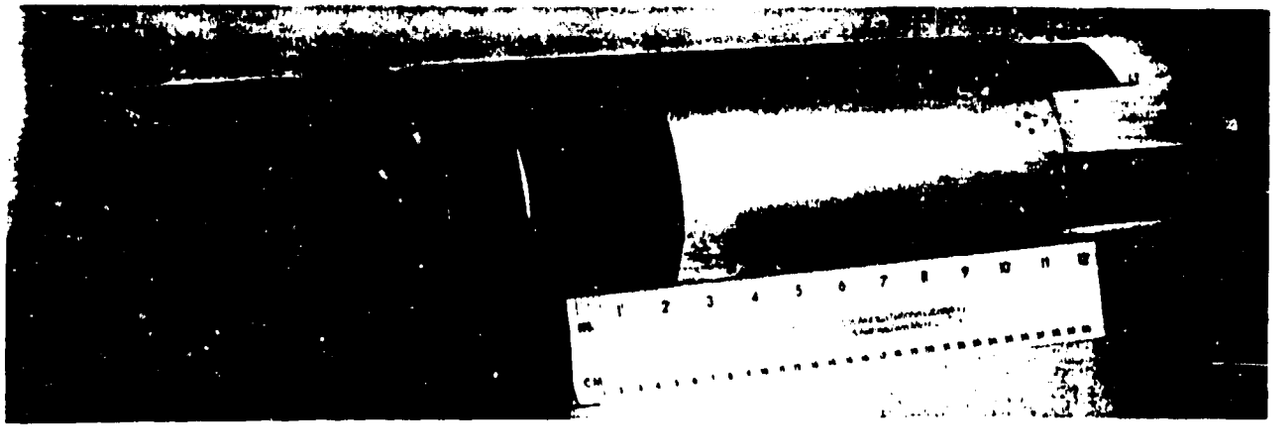

Figure 4. Blast shield test "mock " missile showing microwave reflector.

2.2 USE OF A SINGLE STEEL DISK AS BLAST SHIELD

For use in another missile design, we also investigated the use of a single steel disk as a blast shield. A reproduction of the radiograph of the static test configuration is shown in Fig. 9. An ITOW was used as a surrogate for the precursor warhead. The "donut" seen on top of the steel disk is a high-pressure gas bottle used for a Joule-Thompson cooler for the infrared detector on the actual missile. This high-pressure bottle was used in the test because it is part of the blast shield system. Figure 10 shows the condition of the assembly several hundred microseconds after detonation of the precursor warhead. Little deformation of the blast shield is seen. In fact, radiographs taken at later times in subsequent tests of this configuration show that we are observing the maximum deflection in Fig. 10, and that the blast shield actually springs back toward its original shape at a later time. Note also that debris from the Precision Initiation Coupler (PIC) assembly of the ITOW has hit the high-pressure gas bottle. Figure 11 shows the results of a PINON hydrocode calculation overlaid on the radiograph of Figure 10. The agreement is excellent. Note that the calculation has accurately predicted the folding of the missile skin just below the blast shield mounting station, and the impingement of debris from the PIC on the high-pressure gas bottle. This result gave us confidence in using code calculations for detailed design of the blast shield system.

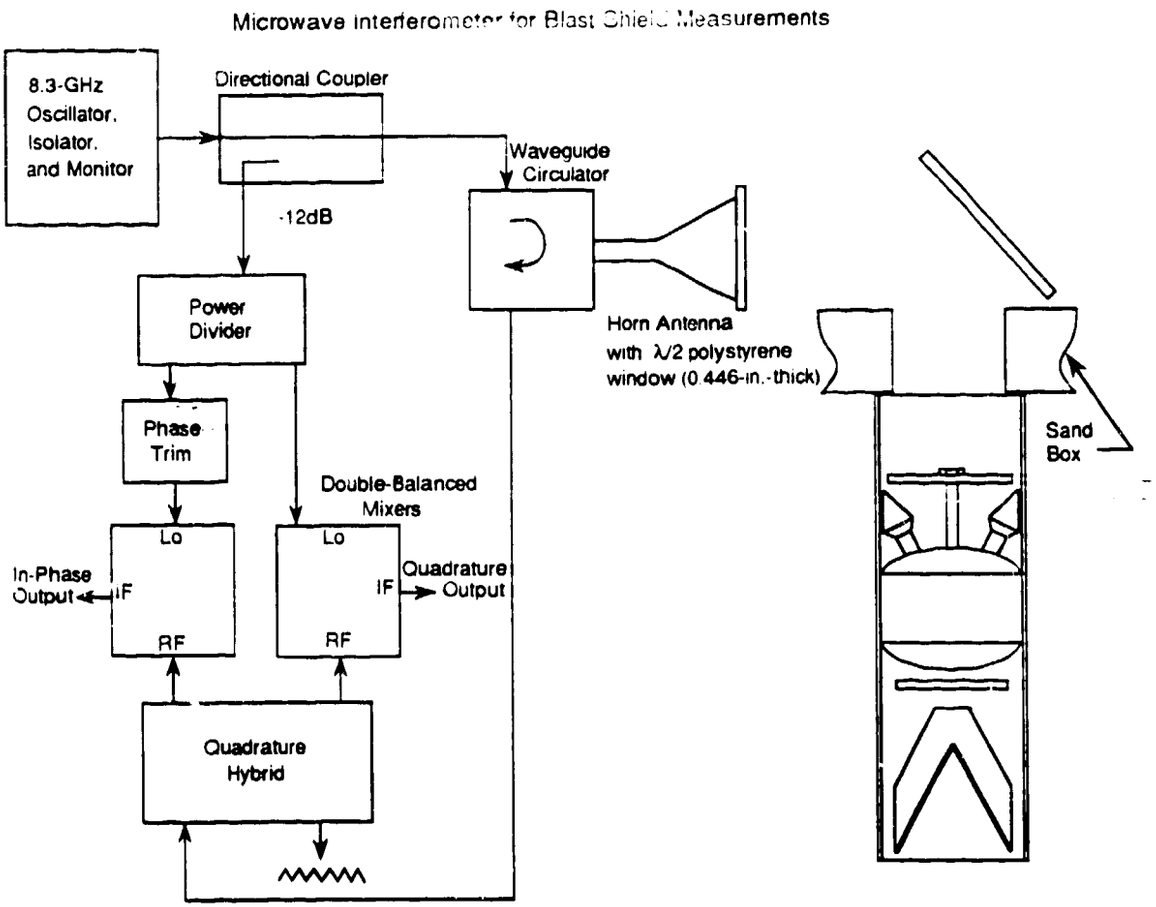

Figure 5. Microwave interferometer for blast shield movement experiments.

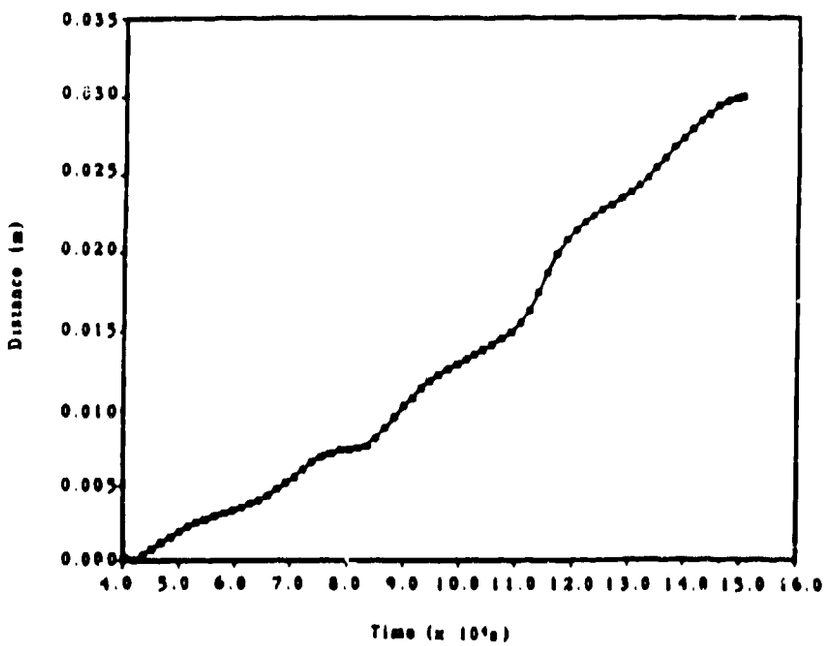

Figure 6. TOW motor displacement, as determined from microwave interferometer.

Figure 7. Triple-exposure radiograph showing TOW motor integrity and position.

Figure 8. 2.3-MeV radiograph showing the efficacy of the TOW motor as a blast shield.

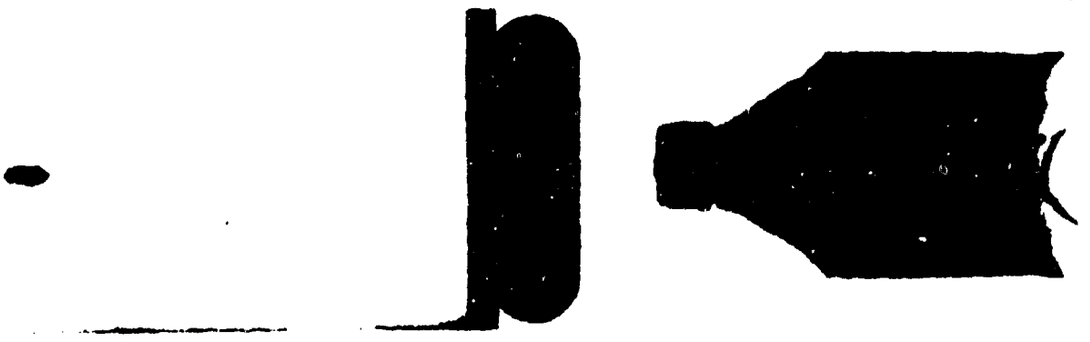

Figure 9. Setup record of the test arrangement using a shaped-steel disk as the blast shield.

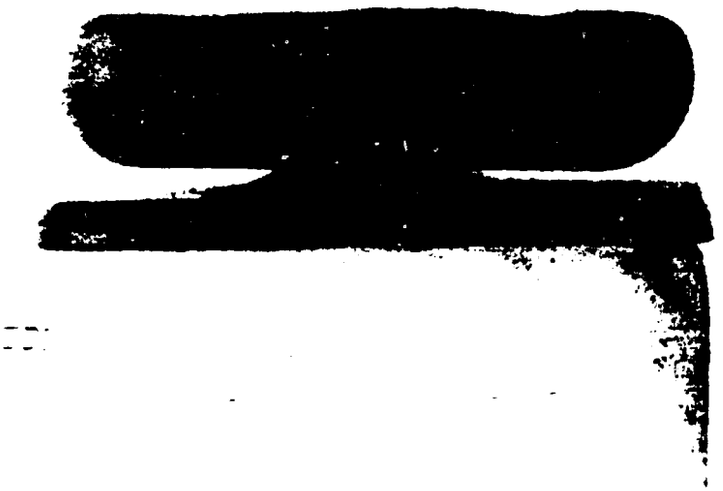

Figure 10. Reproduction of the radiograph of the blast shield and high-pressure gas bottle several hundred microseconds after detonation of the precursor warhead.

Figure 11. Comparison of PINON hydrocode calculation with the experimental results shown in Fig. 10.

3. DYNAMIC SLED TRACK TESTING OF TANDEM WARHEAD SYSTEMS

3.1 SLED TRACK CONFIGURATION

The Los Alamos sled track is 1000 ft long. The sled can be launched from any position along the rail. The usual launch point is 800 ft from the target end of the rail. In its present configuration, the sled has carried payloads of up to 78 lbs to velocities of between 328 ft/s and 1090 ft/s (Mach numbers of 0.29 to 0.95). Any range target can be accommodated, including those with multiple reactive packs. We have tested shaped-charge warheads up to 7-in. diameter. Any liner material also can be tested. Both direct attack and fly-over shoot-down configurations can be tested. Missile dive and pitch angles can be simulated by adjustment of target obliquity and mounting angle of the warhead package on the sled frame.

3.2 DIAGNOSTICS

Timing, firing, and diagnostic equipment include the following: one Hewlett-Packard 2.3-MeV flash x-ray unit, two Hewlett-Packard 450-keV flash x-ray units, 40 channels of 1 ns to 99 s (± 3-ns-accuracy) time interval meters (TIM), 10 channels of 1 ns to 99 s (± 3-ns-accuracy) digital delay units (DDUs), three high-speed (10,000 frames/s) movie cameras, and four independent capacitive discharge units (CDUs) that provide the high-voltage pulse to detonate the warheads. In general, the two 450-keV x rays are used to take radiographs of the precursor and main jets in the reactive packs of the target, and the 2.3-MeV x ray is used to take a radiograph of the main warhead at or shortly after detonation. Both the TIMs (personal communication, Martin, A. D., 1988, Los Alamos National Laboratory Group M-8) and the DDUs, (Martin, 1988) are Los Alamos designed and constructed. Near-term additional diagnostics include a Maxwell Laboratories 8-MeV flash x-ray (PIXY) machine, which is due to become operational in August of 1990. A Cordin Model 330A combination rotating-mirror streak and framing camera has just become operational.

3.3 SLED AND "MOCK" MISSILE ASSEMBLY

The sled assembly is shown in Fig. 12. Variants of the design allow use of from one to four 2.75-in.-diameter Mighty Mouse rocket motors, and one or two 5-in.-diameter HVAR rocket motors. For safety reasons, there is no power aboard the sled. Four knife blades are used for transferring power to the sled; two are for the circuit for each warhead. These blades cut the screens of two individual screen boxes at the target end of the track, thus providing electrical contact to the warhead detonators. An additional knife blade is used to cut a foil make/break switch to provide a time fiducial when the precursor has reached the proper standoff from the target. Sled velocity is measured using Hall-effect transducers located along the side of the rail. A magnet mounted on the side of the sled triggers the transducer as it passes over the transducer. A pulse is sent to a dedicated TIM when each transducer is triggered. The resultant time-vs-position data are differentiated to yield velocity-vs-position values.

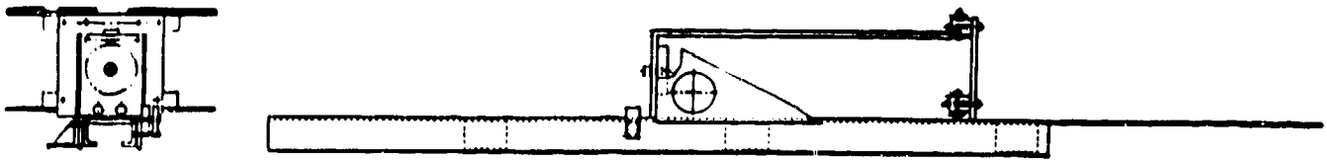

Figure 12. Rocket sled assembly.

A typical "mock" missile used for testing developmental warheads and configurations is shown ready to be mounted to the sled in Fig. 13. Each warhead and the TOW motor and foam blast shield are cemented into individual cylindrical sections of 6-lb/ft^3 foam. The foam, in turn, is cemented into a section of 8-in.-o.d. by 0.072-in.-wall aluminum tube. The three aluminum tube sections are bolted together by means of aluminum connecting rings. The assembly is attached to the sled frame with threaded rods attached to the two connecting rings and the two tube end-section rings. The sled and warhead assembly ready for launch are shown in Fig. 14. We are also capable of testing fielded missile and warhead systems against advanced armors. Figure 15 shows a Hellfire missile mounted on the sled ready for test.

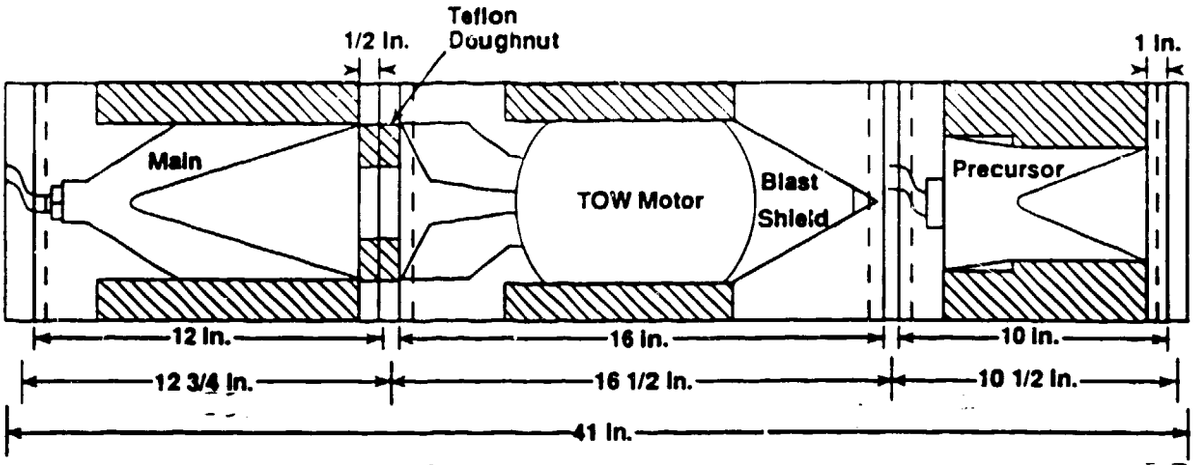

Figure 13. Typical "mock" missile configuration used for sled developmental tandem warhead tests.

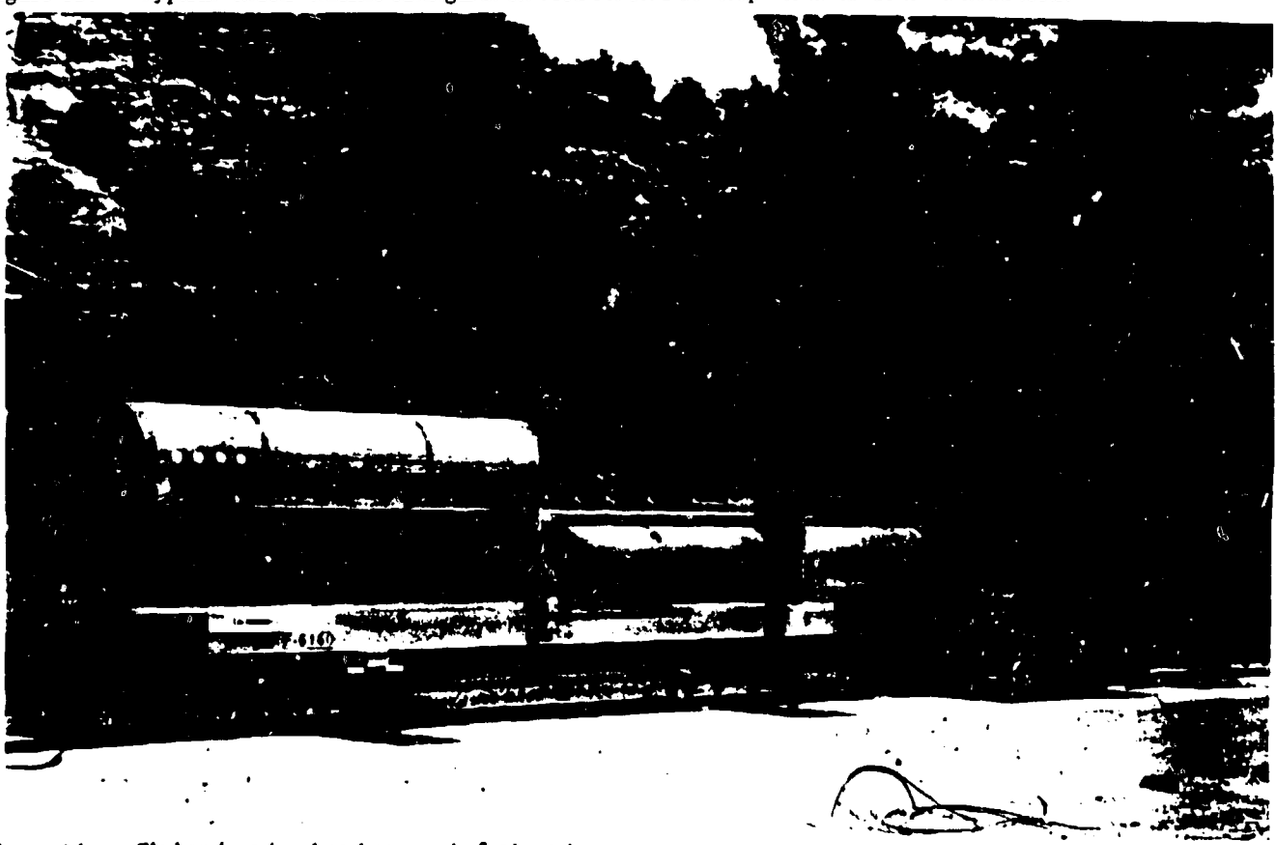

Figure 14. Sled and warhead package ready for launch.

3.4 SYSTEM OPERATION

The operation of the entire sled track system and diagnostics is illustrated in the functional flow diagram shown in Fig. 16. The fire button triggers DDU channels, which start the high-speed cameras before triggering the low-voltage CDUs that ignite the rocket motor(s). As the sled approaches the target end of the track, the four knife blades used to detonate the warhead cut into the screens of the screen box. When the precursor warhead reaches the proper standoff from the target, the additional knife blade cuts the trigger foil switch mounted on top of the right screen box. The foil switch is powered from a Model DM 10 VSM Velocity Screen Monitor (personal communication, Martin, A. D., 1988, Los Alamos National Laboratory Group M-8). When the foil switch is broken (or shorted) by the knife blade, the VSM sends out a 20-V pulse that triggers CDU #1, which fires the precursor warhead and causes the TIMs to start counting, the additional DDU channels to trigger the x-ray units at the preset delay times, and the DDU channel to set the time delay for

triggering CDU #2, which detonates the main warhead. Foil time-of-arrival (TOA) switches, identical to the trigger foil switch, are placed in the target to measure the time at which the precursor jet reaches the target, the time at which the reactive packs detonate, and the jet penetration velocity. Operation of the TOA switches is the same as for the trigger foil switch, except that now the VSM sends a pulse to the stop on the TIM. The x rays may also be triggered from the break (or short) time of a TOA switch. For this case, the VSM sends a pulse to the DDU, which sets the delay to trigger the x-ray unit. As with the foil TOA switches, the times for the piezoelectric pressure pin switches and for ionization pin switches can also be recorded on the TIMs.

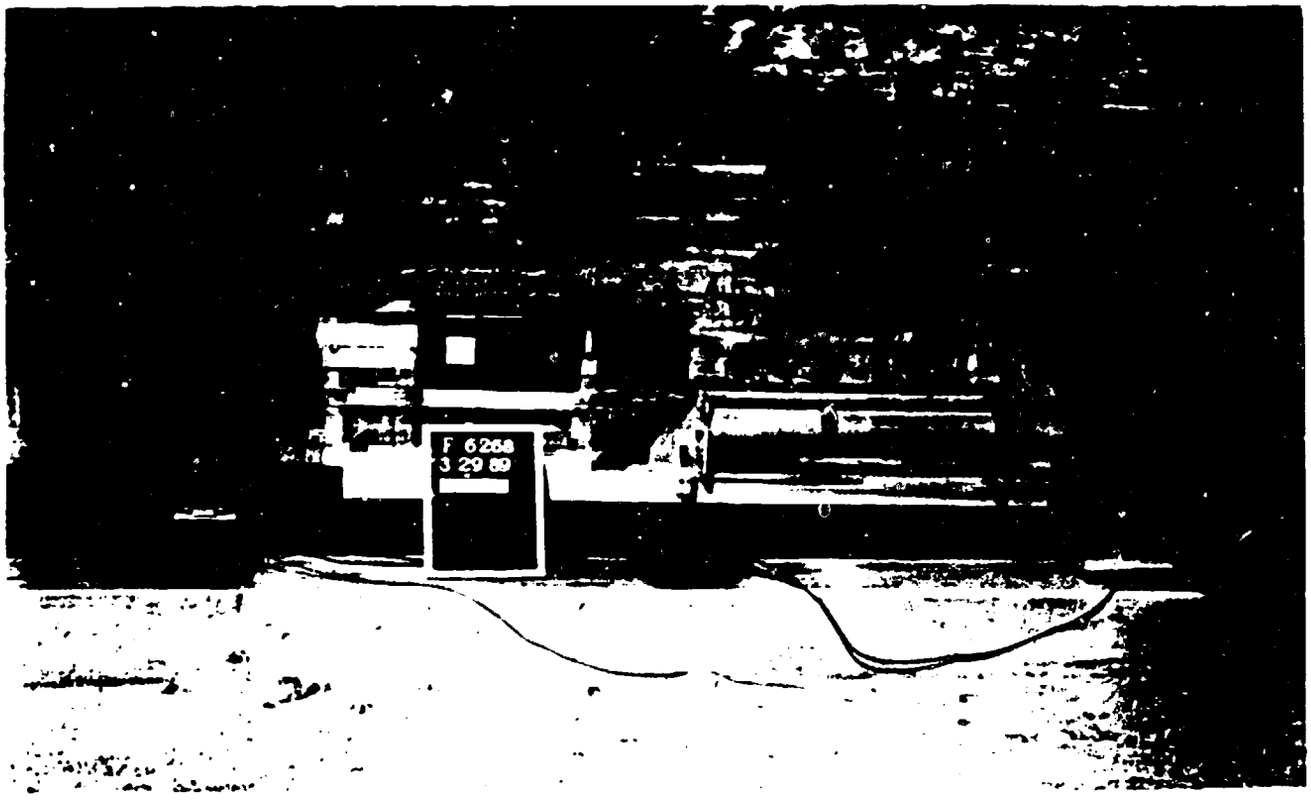

Figure 15. Hellfire missile ready for launch.

4. TYPICAL EXPERIMENTAL RESULTS FROM SLED TESTS OF TANDEM WARHEADS

4.1 DIAGNOSTIC REQUIREMENTS

Because this paper is unclassified, detailed performance results of specific warhead configurations against specific armors cannot be presented. However, it is important to note that our experiments have illustrated the need for extensive diagnostics to properly analyze the dynamics of the warhead-target interactions. We found that the sole use of TOA switches, ionization pins, and terminal observation of the armor plates recovered after the shot can lead to ambiguous and sometimes erroneous conclusions. We found that the use of a visualization technique, such as the extensive use of flash radiography, is essential for adequate interpretation of experimental results.

In the discussion of the blast shield studies, we have already seen an application of flash radiography as a valuable diagnostic in static tests (Figs. 7 and 10). We have also used flash radiography as a primary diagnostic on dynamic sled tests of full-up tandem warhead assemblies. Analysis of these radiographs provides valuable insight into the jet-target interactions. The possible extent of interactions between the target and the missile is illustrated in Fig. 17, which is a 2.3-MeV x ray of the main charge and TOW motor taken 100 μs after the main warhead detonates. The tamper plate from the first reactive pack has impacted the TOW motor. The jet with its spall bubole can be clearly seen exiting the TOW motor and tamper plate.

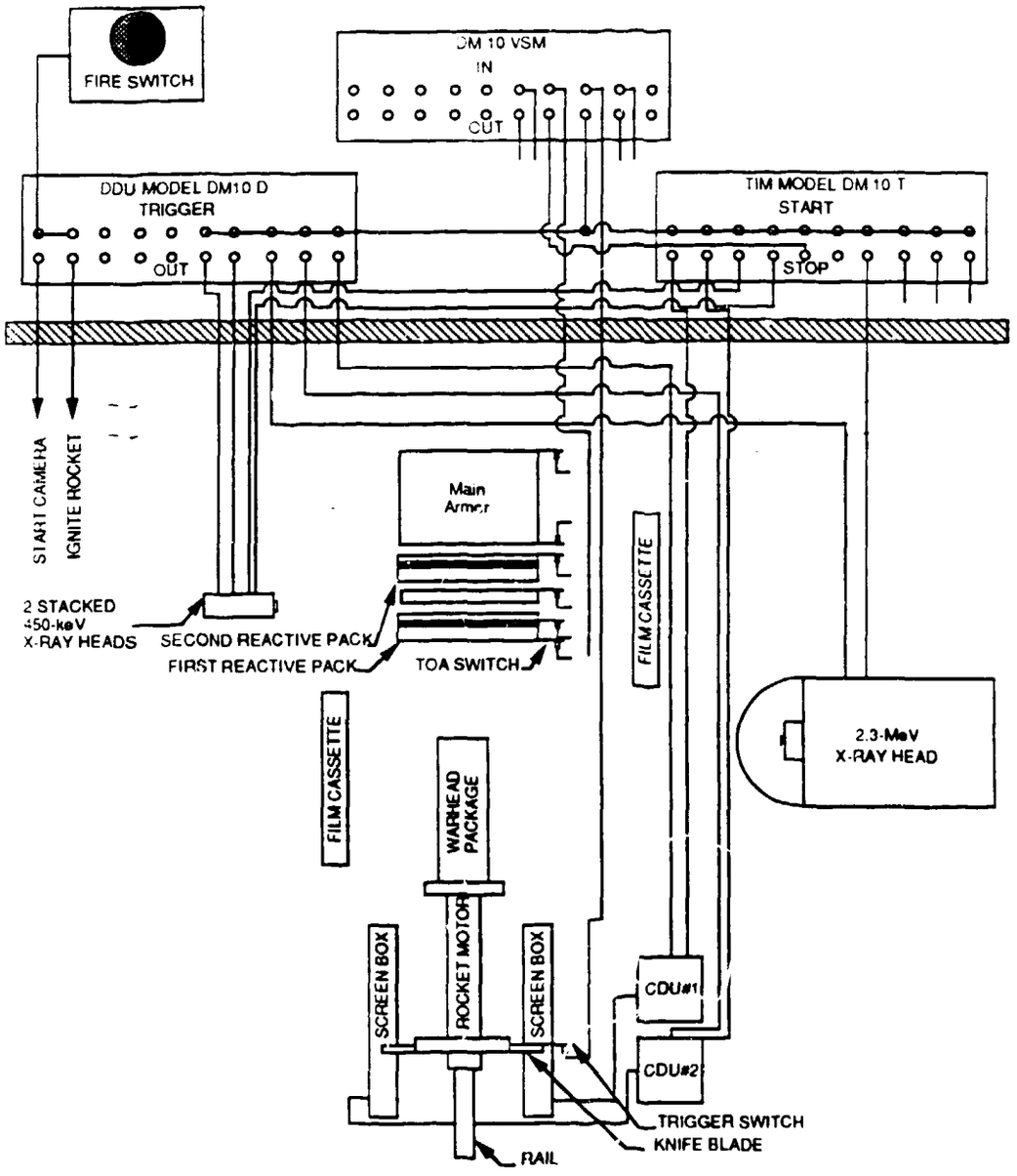

Figure 16. Functional flow diagram for sled track and diagnostic operation.

4.2 DYNAMIC JET-TARGET INTERACTIONS

An example of jet-target dynamic interactions is afforded by comparing the results of the radiographs in Figs. 18 and 19. Figure 18 shows a 2.3-MeV radiograph taken 100 μs after main warhead detonation. The main jet has passed through the TOW motor and is about to strike the upper edge of the flying first-reactive-pack tamper plate. In this shot, we did not defeat the target. We believe the main jet was severely disrupted by the tamper plate. Based on this result, we repeated the shot but increased the time delay between the precursor detonation and main warhead detonation to allow the tamper plate to clear the shot line. Figure 19 shows radiographs from this test. The top image is the 2.3-MeV x ray showing that, indeed, the main jet is now clearing the tamper plate. The bottom image is a double-exposure 450-keV radiograph. From the first exposure, the lower image, we infer that the precursor has ignited the first reactive pack because the two leftmost plates in the picture are only beginning to fly apart. The second exposure, the upper image, shows a still well-formed main jet.

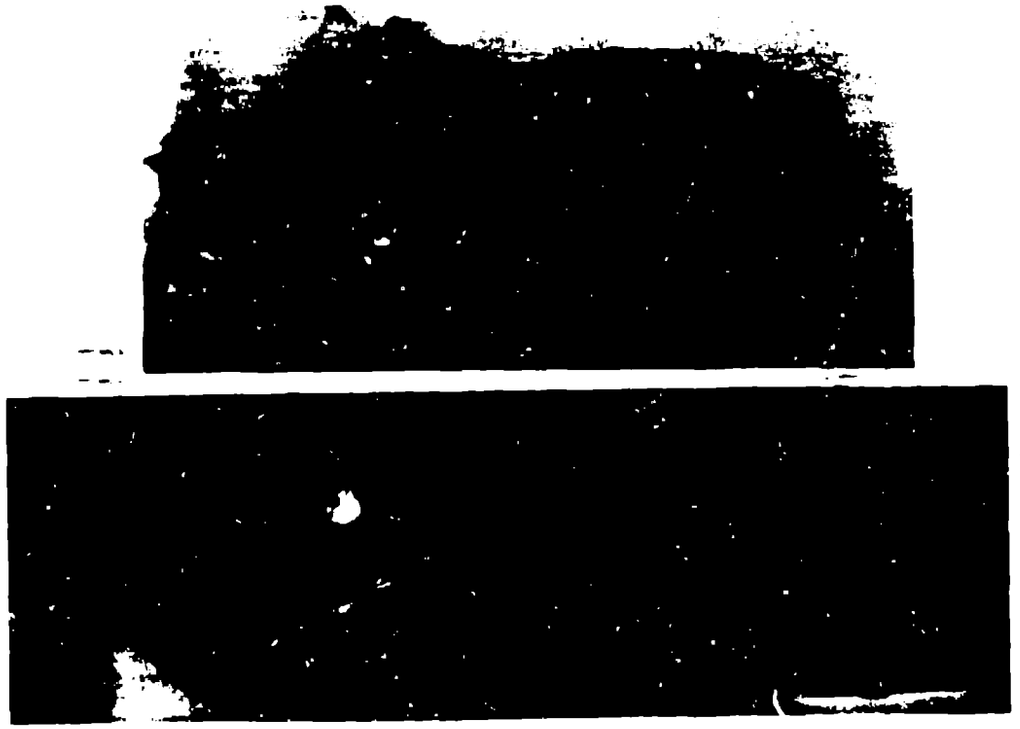

Figure 17. Photograph of a 2.3-MeV radiograph showing tamper plate impacting TOW motor.

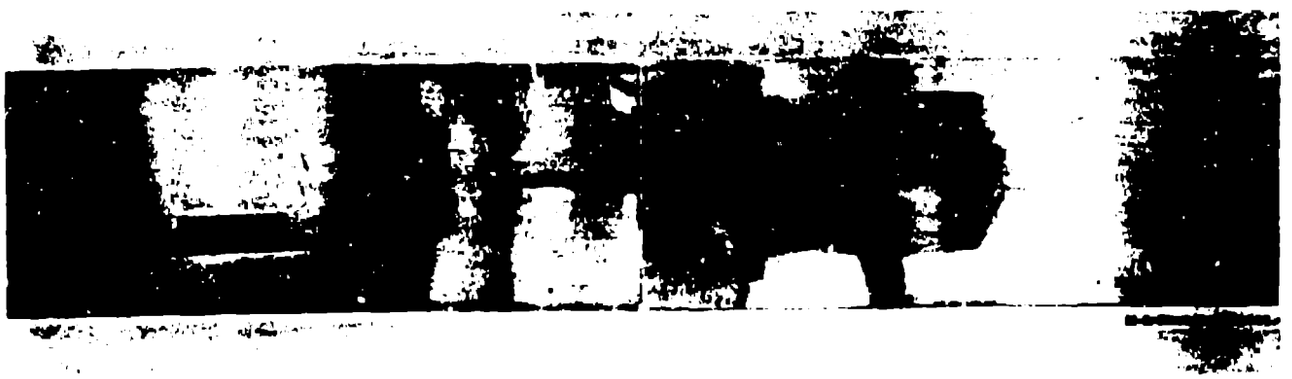

Figure 18. Photograph of a 2.3-MeV radiograph showing the main jet about to hit the tamper plate.

We have also used flash radiography to study the effectiveness of various precursors in detonating multiple reactive packs in armor of the type shown in Fig. 1. For example, the lower image of the double-exposure 450-keV x ray in Fig. 19 shows that the precursor jet has ignited the first reactive pack. The second exposure, the upper image that is taken sometime later, shows that the precursor also ignited the second reactive pack: the two darker, separated plates are in the lower-right portion of the picture. This result verifies the conclusion reached from the TOA switches located on the second reactive pack. These times were 151.7 μs after detonation of the precursor for the switch located on the front of the second reactive pack, and 213.5 μs after detonation of the precursor for the switch located on the back of the second reactive pack. Both these times are well before the main warhead is detonated. In Fig. 20, a case is shown in which the precursor jet ignited the first reactive pack but failed to detonate the second reactive pack. The first exposure, top image, shows the first reactive pack as the lighter image at the far left; the second reactive pack is the lighter, rectangular objects in the center of the picture. The second exposure shows that the first reactive plate is gone, but the darker, rectangular object in the center of the picture is the second reactive pack, which has still not begun to separate. The main jet can be seen entering from the left side. The switch data in this case were inconclusive; the switches triggered well after they should have, if the precursor ignited the second reactive pack, but still well before the main warhead detonated.

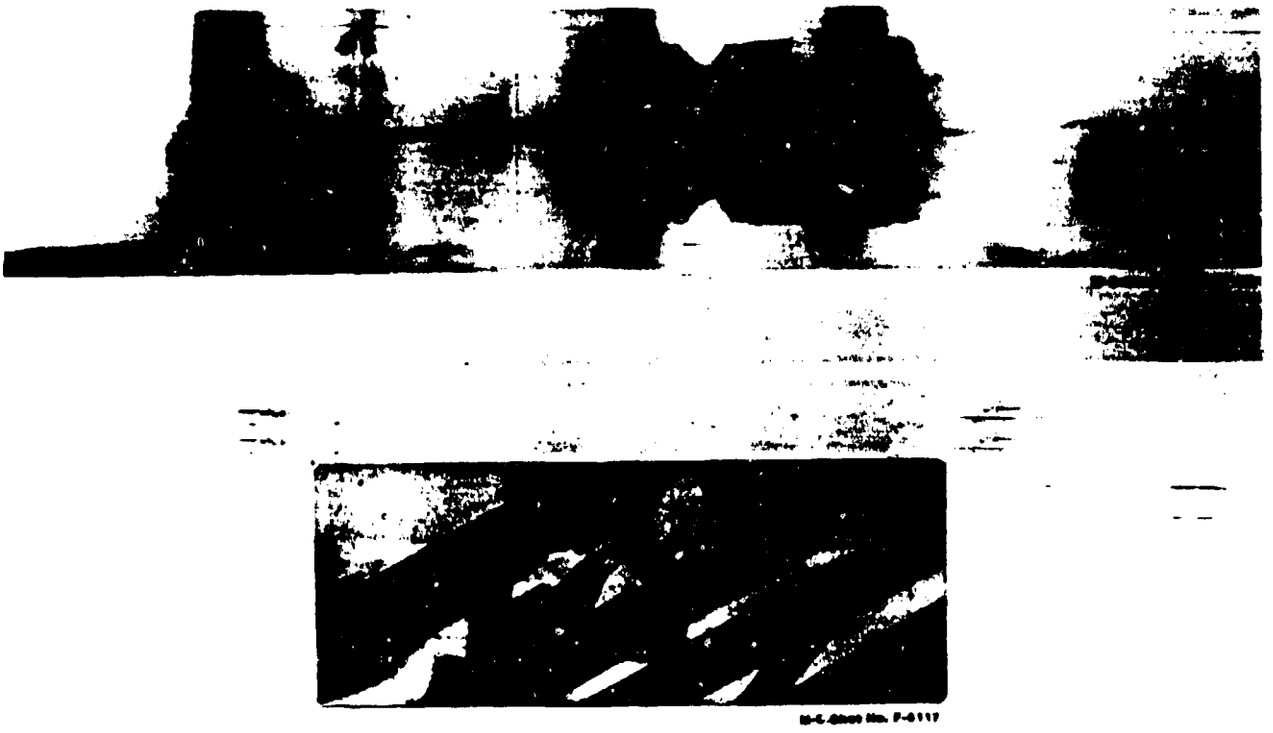

Figure 19. *Top*: 2.3-MeV radiograph showing main jet clearing the tamper plate.
Bottom: Double-exposure 450-keV radiograph showing that the precursor detonated both reactive packs, the precursor jet exited the stripper plate, and the main jet was about to enter the broken stripper plate.

Figure 20. Reproduction of the 450-keV x ray showing that the precursor did not detonate the second reactive pack.

We now present an interesting example of the necessity of sophisticated diagnostics in analyzing the performance of tandem warheads against multiple-reactive-pack armors. In this test, the precursor jet used a copper liner and the main jet a tantalum liner. The target was not defeated. The switch data indicated that the precursor did not detonate the second reactive pack. However, both the flyer and tamper plates from the second reactive pack were recovered after the shot. The tamper plate had a very large hole with two distinct lobes through it, indicating that both the precursor and the main jet had penetrated it. The flyer plate had two distinct large holes through it, confirming that both jets had penetrated it. From the size of the holes, it was hard to imagine that the precursor jet did not ignite the reactive pack. Both the tamper plate and the flyer plate from the first reactive pack were also recovered. In the tamper plate was a hole through its middle. The flyer plate had a hole through its midpoint, and a long slot at the top. Thus the preponderance of evidence was that the precursor had indeed ignited both reactive packs, and the main jet notched the front flyer plate. The single-exposure 450-keV x-ray shown in Fig. 21 shows that the precursor did not detonate the second reactive pack. Then how do we explain the two large holes through the second reactive pack? We sent the plates for testing by x-ray fluorescence spectroscopy of the material on the edges of the holes. The material in both holes in the second reactive pack flyer plate contained only tantalum. No

copper above the level in a blank steel sample was detected. The material in the hole in the first reactive pack tamper plate was copper. No tantalum was detected. Thus the copper precursor jet ignited the first reactive pack but not the second. The tantalum main jet bifurcated and detonated the second reactive pack.

Figure 21. 450-keV x ray shows precursor did not detonate the second reactive pack.

4.3 FAILURE ANALYSIS

An example of the use of flash radiography for failure analysis is afforded by the 2.3-MeV radiograph shown in Fig. 22. The records from the 450-keV x ray and the TOA switches showed that the precursor did not penetrate the first reactive pack. Figure 22, taken 135 μs after the main warhead detonated, shows the main warhead jet penetrating the igniter tube of the TOW motor. It also shows that the precursor warhead did not detonate. The precursor is not in the proper axial position in the assembly. It should have been several inches farther forward. It has slid back in its mounting during the sled ride, and the detonator appears to have been broken off the back of the charge when it hit the tip of the foam blast shield. As a result of this determination, we redesigned the precursor warhead mounting. A subsequent test of the redesigned configuration was successful.

Figure 22. 2.3-MeV x ray showing undetonated precursor warhead.

5. CONCLUSIONS

We demonstrated the ability to integrate a variety of diagnostics with a dynamic sled track test facility to study tandem warhead jet-target dynamic interactions. The necessity of using multiple diagnostics, including flash radiography, to properly diagnose the performance of tandem warhead anti tank missile systems against multiple-reactive-pack armors has been demonstrated. Our tests show that the precursor warhead must detonate all the reactive packs for good performance against the targets. In many tests, we have seen significant differences between the dynamic sled track tests and static tests of the same configuration. We conclude that more dynamic-static test comparisons need to be performed to understand the reasons for the observed differences.

REFERENCES

McCall, G. H., Bongianni, W. L., and Miranda, G. A., 1985: Microwave Interferometer For Shock Wave, Detonation, and Material Motion Measurements, Rev. Sci. Instrum., 56, 8.

Martin, A. D., 1988: Digital Delay Unit, U.S. Patent # 4,719,375, January 12, 1988.